Multibeam Focal Plane Arrays With Digital Beamforming for High Precision Space-Borne Ocean Remote Sensing

Oleg A. Iupikov, *Member, IEEE*, Marianna V. Ivashina, *Senior Member, IEEE*, Niels Skou, *Fellow, IEEE*, Cecilia Cappellin, Knud Pontoppidan, and Cornelis G. M. van 't Klooster, *Senior Member, IEEE*

***Abstract*— The present-day ocean remote sensing instruments that operate at low microwave frequencies are limited in spatial resolution and do not allow for monitoring of the coastal waters. This is due to the difficulties of employing a large reflector antenna on a satellite platform, and generating high-quality pencil beams at multiple frequencies. Recent advances in digital beamforming focal-plane arrays (FPAs) have been exploited in this paper to overcome the above problems. A holistic design procedure for such novel multibeam radiometers has been developed, where: 1) the antenna system specifications are derived directly from the requirements to oceanographic surveys for future satellite missions and 2) the numbers of FPA elements/receivers are determined through a dedicated optimum beamforming procedure minimizing the distance to coast. This approach has been applied to synthesize FPAs for two alternative radiometer systems: a conical scanner with an offset parabolic reflector and a stationary wide-scan torus reflector system, each operating at *C*-, *X*-, and Ku-bands. Numerical results predict excellent beam performance for both systems with as low as 0.14% total received power over the land.**

***Index Terms*— Array antennas, microwave radiometers, reflector antenna feeds.**

I. Introduction

MICROWAVE radiometry is a highly versatile method of remote sensing, capable of delivering measurements of a variety of geophysical properties of the ocean and atmosphere, even through clouds. The retrieval methods distinguish the individual effects of different geophysical properties by using the frequency and polarization state of the microwave radiation detected by the antenna. Despite such versatility, the exploitation of microwave radiometry in Earth observation has been constrained by the difficulties of generating antenna beams with low sidelobes and cross-polarization, and accomodating several feeds operating at different frequencies, when deploying the antenna on a satellite platform [1]. In particular, for high resolutions demanded by oceanographers, the current antenna designs would need to be scaled up to a physical size that is too large to be achievable or affordable within typical Earth observation infrastructure budgets. For this reason, space agencies have been seeking solutions to overcome what seems at present to be an unpassable barrier to further significant improvement of a whole class of remote sensing methods.

The European Space Agency (ESA) is currently considering the ocean missions where extreme weather, climate variability, and coastal and marginal-ice-zone studies are strong drivers [2], [3]. These studies require a very high radiometric resolution, i.e., around 0.25 K, and at the same time a high spatial resolution approaching 20 km at C- and X-bands and 10 km at Ku-band (see Table I) [4]. This desired performance represents a significant improvement compared with existing space-borne radiometer systems, such as AMSR-E and WindSat [5], [6]. They feature spatial resolutions around 55, 35, and 20 km at the C-, X-, and Ku-bands, and the radiometric resolution provided by AMSR-E is 0.3 K at the C-band and 0.6 K at the X- and Ku-bands, while for WindSat it is around 0.7 K. Moreover, future systems are required to provide valid observations up to very short distances from the coastline, i.e., 5–15 km, while the existing systems can observe only up to $\sim$100 km.

It can be shown that the desired spatial resolution calls for a reflector antenna with $\sim$5 m aperture diameter [7] that is very challenging considering the experience of Soil Moisture Active Passive (SMAP) mission, which has a 6 m reflector [8], [9]. On the other hand, for all three frequency bands, the bandwidths are limited to a few hundreds of MHz that makes it possible (at least in theory) to achieve very low noise temperatures of the receivers. However, even the most optimistic receiver noise properties cannot ensure the required radiometric resolution when considering a single beam scanning system [see Fig. 1(a)]. For a scanner, the only solution is to employ

Manuscript received August 1, 2016; revised August 22, 2017; accepted October 4, 2017. Date of publication October 16, 2017; date of current version February 1, 2018. This work was supported in part by the framework of the Advanced Multi-Beam Radiometers Project that is a collaborative effort between TICRA, DTU-Space (Denmark), HPS (Germany), and Chalmers, in part by the European Space Agency (contract 4000107369-12-NL-MH), in part by the Swedish Research Council, and in part by the Swedish National Space Board grants. *(Corresponding author: Oleg A. Iupikov.)*

O. A. Iupikov and M. V. Ivashina are with the Signals and Systems Department, Chalmers University of Technology, 41296 Gothenburg, Sweden (e-mail: oleg.iupikov@chalmers.se; marianna.ivashina@chalmers.se).

N. Skou is with the DTU-Space, Technical University of Denmark, 2800 Kgs. Lyngby, Denmark (e-mail: ns@space.dtu.dk).

C. Cappellin and K. Pontoppidan are with TICRA, 1119 Copenhagen, Denmark (e-mail: cc@ticra.com; kp@ticra.com).

C. G. M. van 't Klooster was with the European Space Agency, European Space Research and Technology Centre, 2200 AG Noordwijk, The Netherlands. He is now with the Eindhoven University of Technology, 5600 MN Eindhoven, The Netherlands (e-mail: kvtklooster@gmail.com).

Color versions of one or more of the figures in this paper are available online at http://ieeexplore.ieee.org.

Digital Object Identifier 10.1109/TAP.2017.2763174

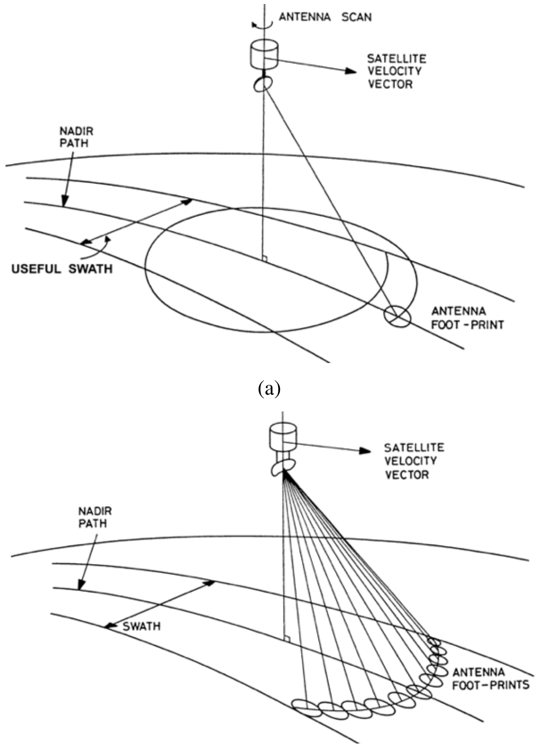

Fig. 1. Operational principle of (a) conical scan and (b) push-broom microwave radiometers for ocean remote sensing.

several independent beams per frequency and improve radiometric resolution by integrating several footprints (FPs). This calls for a large number of overlapping beams—in the present case up to 30 beams at the Ku-band. An alternative is a push-broom system [10], [11], where many beams cover the swath simultaneously, as shown in Fig. 1(b). Using traditional feeds, each antenna beam is associated with its own receiver, and high radiometric resolution is achieved thanks to the fact that the signals associated with multiple across-track FPs do not have to be multiplexed through a single receiver. Radiometric resolution is no longer a problem, but a more complicated antenna design (a tilted parabolic torus reflector) is needed as well as many beams—for the present case up to 156 at the Ku-band. Realizing these, while correcting for the antenna field distortions causing the well-known triangular FPs and their large separation on the Earth [10], [11], represents a great challenge. In addition, the implementation of this concept should be feasible regarding the resource requirements, i.e., the size, mass, and power consumption.

As demonstrated in this paper (see Section IV), the above radiometric requirements cannot be fulfilled by using traditional cluster feeds of horns (in one-horn-per-beam configuration), employed at such multifrequency radiometer antennas. Recent studies initiated by ESA [12]–[15] have identified a promising solution that originates from the field of radio astronomy [16]–[22], where instrument designs have evolved to meet the high-sensitivity and large-coverage requirements of ground-based observatories exploring the universe without the above challenges. This solution is based on "dense" focal plane arrays (FPAs), where many small antenna elements take part in the formation of each beam (so that each beam can be optimized for high performance, even far off-axis beams) and the same element takes part in the formation of multiple beams (so that the FPs overlap), thanks to digital beamforming. Dense FPAs capable of generating multiple beams find their application not only in radio astronomy, but also in telecom applications, where they are referred to as multibeam antennas in multifeed per beam (MFB) configuration. The technology used in space for telecom MFB applications is mature and typically used for multibeam missions in the L-band, see for example the Thuraya satellite [23] and the Inmarsat satellites [24]. For example, Thuraya employs an L-band 128-element dipole array feeding a 12.25×16 m mesh transmit–receive reflector, and generates more than 200 pencil beams that can be redirected on-orbit [23]. Recent developments have been made for MFB applications in the Ka-band, where [25]–[27] have developed compact and high efficient feed arrays made by closely spaced horn antennas excited by a beamforming network. It is noted that MFB antennas for telecom applications are located on the geostationary orbit and are driven by requirements which differ from the ones for radiometric applications treated in this paper.

The requirements for radiometer systems will be discussed in Section II, and translated into antenna system specifications and beam characteristics to optimize for. The reflector antenna geometries used in this paper are briefly described in Section III. Section V will cover the synthesis of FPAs for such systems, and include the following original contributions: 1) a dedicated optimum-beamforming algorithm minimizing the distance to coast; 2) optimized antenna patterns and radiometric parameters—as obtained for the half-wavelength dipole element FPAs—that fulfill all above requirements with almost twice less elements in comparison to the conventional conjugate-field-matching optimization approach [12]; and 3) validation of the simplified array model with the assumed identical embedded element patterns (EEPs) [12], [14] across the full MoM model for the purpose of the FPA synthesis. Finally, digital receiver resource requirements will be considered in Section VI.

II. From Oceanographic Requirements to Antenna System Specifications

The requirements for future missions in Table I are defined in terms of performance metrics for oceanographic surveys, i.e., spatial resolution, radiometric resolution, bias, and distance to coast. Since these terms are not commonly known by antenna designers, next we will summarize their definitions and use these to derive the antenna system specifications.

A. Spatial Resolution (FP) $\Rightarrow$ Reflector Diameter

The radiometer spatial resolution is defined by the FP, which is the area on the Earth surface bounded by the projection of the radiation pattern at -3 dB level. Sometimes the FP size along track is of importance (when, e.g., the scan rotation rate should be calculated) and sometimes we discuss the FP across track (when, e.g., the radiometer sampling rate should be

TABLE I

RADIOMETRIC REQUIREMENTS FOR FUTURE OCEAN MISSIONS

Freq., [GHz]	Band width, [MHz]	Polari-zation	Radiometric resolution, [K]	Bias, [K]	Spatial resolution, [km]	Dist.to coast, [km]
6.9	300	V, H	0.30	0.25	20	5-15
10.65	100	V, H, S_3, S_4	0.22	0.25	20	5-15
18.7	200	V, H, S_3, S_4	0.25	0.25	10	5-15

found). But in order to compare different radiometric systems, it is convenient to have one number as a figure of merit that can be an arithmetic [like in (1)] or geometric mean of the FP size along and across tracks.

The required spatial resolution in Table I is defined in terms of the average FP size on the Earth's surface

$$\mathrm{FP} = (Y \times \theta_{3\mathrm{dBT}} + Y \times \theta_{3\mathrm{dBL}}/\cos\nu)/2 \tag{1}$$

where $\theta_{3\mathrm{dBL}}$ and $\theta_{3\mathrm{dBT}}$ are the half-power beamwidths of the antenna main beam along the elevation ("along track") and azimuth ("across track") directions, respectively, expressed in radians; ν is the incidence angle as measured from the normal to the Earth's surface and Y is the distance from the satellite to the observation point on the Earth.

The FP is directly related to the antenna beamwidth, and hence determines its aperture diameter. This diameter should be at least 5 m for the present case ($\nu = 53^\circ$ and $Y = 1243$ km) in order to realize the FP of 20 km at the C-band. Since for the considered system, the same antenna is used at different bands, and the same FP cannot be obtained at both C- and X-bands. The required FP shall, therefore, be considered a guideline, and values both slightly above and below can be acceptable. The important factor is that the beam crossover points should be at the -3 dB level. This means that if the FP is reduced, more beams are needed to cover a particular region on the Earth.

B. Bias (ΔT) $\Rightarrow$ Acceptable Cross-Polarization Power

Bias is a systematic error of the measured brightness temperature of the sea. For full polarization radiometers, ΔT is typically driven by polarization leakage. The approximate values of the sea temperature for the incidence angle 53° are $T_v = 150$ K and $T_h = 75$ K in vertical and horizontal polarizations, respectively. To measure T_h, one can select the copolar component as the horizontal polarization. The cross-polarization component of the pattern, however, will pick up the vertical component of the radiation from the sea, which has a temperature of 150 K. Using the assumption that the amount of radiation received from the sky is negligible, it is sufficient to consider the antenna pattern in the angular region covering the Earth only, and hence compute the total temperature as $T_b = T_v P_{\mathrm{cross}} + T_h P_{\mathrm{co}}$, where P_{co} and P_{cross} are the copolarization and cross-polarization received powers in the angular region of the Earth, normalized to the total field power ($P_{\mathrm{co}} + P_{\mathrm{cross}}$) in the same angular region. Then, ΔT

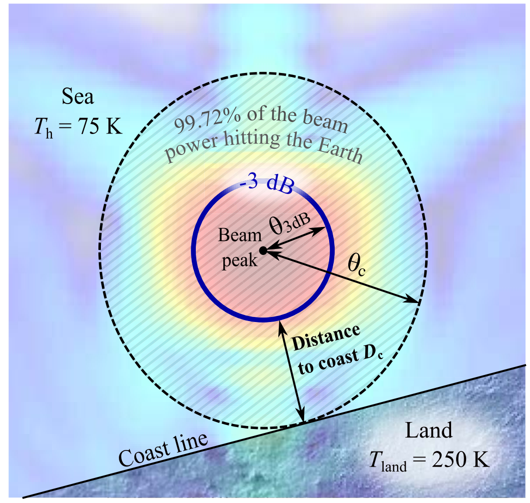

Fig. 2. FP falling on the sea near a coast: illustration for the definition of the distance to coast D_c.

can be found as

$$\Delta T = T_b - T_h = (T_v - T_h)P_{\mathrm{cross}} \tag{2}$$

where P_{cross} is the acceptable relative cross-polarization power of the antenna pattern that covers the Earth. Using (2), one can show that the requirement for $\Delta T = 0.25$ K can be satisfied only if P_{cross} does not exceed 0.34%.

C. Bias (ΔT) $\Rightarrow$ Distance to Coast (D_c) = Acceptable SideLobes

Table I states that D_c should be 5–15 km, when measured from the FP. The reason behind this requirement is that the brightness temperature of the land is much higher than that of the sea. This means that the power in the antenna pattern over land must be sufficiently small. In order to assess the influence from the land, the cross polarization can be neglected. The brightness temperature of the land surface is about $T_{\mathrm{land}} = 250$ K. Assuming the measurements at horizontal polarization, the sea temperature is around $T_h = 75$ K. If there is no land below the satellite, the radiometer will receive an amount of power proportional to $T_h P_{\mathrm{co}}$. If the satellite covers both the land and sea regions, the power from the sea is $T_h(P_{\mathrm{co}} - P_{\mathrm{land}})$, where P_{land} is the relative copolarization power in the land region. The signal from the land is $T_{\mathrm{land}} P_{\mathrm{land}}$. The measured temperature and ΔT are, therefore

$$T_b = T_h \frac{P_{\mathrm{co}} - P_{\mathrm{land}}}{P_{\mathrm{co}}} + T_{\mathrm{land}} \frac{P_{\mathrm{land}}}{P_{\mathrm{co}}} \tag{3}$$

$$\Delta T = T_b - T_h = (T_{\mathrm{land}} - T_h)\frac{P_{\mathrm{land}}}{P_{\mathrm{co}}}. \tag{4}$$

We will now determine D_c with the help of Fig. 2, where we have assumed a straight coastline and a circular-symmetric beam with the beamwidth of $\theta_{3\mathrm{dB}}$. The beam is located over the sea and the distance from the peak to the coast is indicated by the angle θ_c, while the power in the cone with semiangle θ_c is denoted by P_c. The power outside this cone is $P_{\mathrm{co}} - P_c$

and approximately half of this power will fall on the land, so we have $P_{\text{land}} = (P_{\text{co}} - P_c)/2$. Substituting this into (4) gives

$$\frac{P_c}{P_{\text{co}}} = 1 - \frac{2\Delta T}{T_{\text{land}} - T_h}. \tag{5}$$

Inserting the required $\Delta T \leq 0.25$ K in (5) gives

$$\frac{P_c}{P_{\text{co}}} \geq 1 - \frac{2 \times 0.25}{T_{\text{land}} - T_h} = 0.9972. \tag{6}$$

Equation (6) shows that the required accuracy is obtained when the coastline is located outside a cone around the main beam containing 99.72% of the total power on the Earth. Hence, in order to reduce D_c, one should minimize this cone. Then, D_c can be defined as the angular difference $\theta_c - \theta_{3\text{dB}}$ projected on the Earth surface, that is

$$D_c = Y \sin\theta_c - Y \sin\theta_{3\text{dB}} \approx (\theta_c - \theta_{3\text{dB}})Y. \tag{7}$$

For nonsymmetric patterns, the same procedure can be used, where the beamwidth $\theta_{3\text{dB}}$ is assumed to be equal to the average beamwidth for all antenna pattern cuts.

It should be noted that due to nonzero incidence angle ν, the shape of the FP stretches in the along-track direction by the factor $1/\cos(\nu)$. Therefore, the distance-to-coast in the along-track direction will also be factor $1/\cos(\nu)$ larger than the calculated one from (7) if the reflector antenna beam is circular symmetric. However, for the present case, the beamformer minimizes D_c, making the beam elliptical with major axis in the across-track direction. This elliptical beam results in an FP close to circular symmetric, and therefore, the initial assumption of a circular antenna beam gives close approximation of the D_c value.

D. Radiometric Resolution (ΔT_{Min}) $\Rightarrow$ Number of Beams

Radiometric resolution is the smallest change in input brightness temperature that can be detected. For a full-polarization radiometer, it can be found as

$$\Delta T_{\text{min}} = \frac{T_{\text{sys}}}{\sqrt{N_b B \tau}} = \frac{T_{\text{rec}} + T_b}{\sqrt{N_b B \tau}} \tag{8}$$

where τ is the integration interval, B is the radiometer effective bandwidth, T_{rec} is the receiver noise temperature, and N_b is the number of beams. Since $T_h \ll T_v$, it is more affected by the erroneous power signal from land.

The required ΔT_{min} can be achieved by making a tradeoff between N_b for a given reflector diameter and complexity of the feed. For a conically scanning antenna, rotating at 11.5 r/min, N_b in the along-track direction is selected such to cover the same strip width on the Earth at each frequency band. To reach the required ΔT_{min}, we need the following:

1) two beams along track at 6.9 GHz;
2) three beams along track and seven beams across track at 10.65 GHz;
3) five beams along track and six beams across track at 18.7 GHz.

For a push-broom case, the antenna is stationary, and its ΔT_{min} is about one order of magnitude better than the one for the scanner. This is at the expense of a very large N_b and correspondingly a large number of receivers. For a swath of 600 km, we need the following:

1) 58 beams across track at 6.9 GHz;
2) 89 beams across track at 10.65 GHz;
3) 156 beams across track at 18.7 GHz.

TABLE II
ASSUMED NOISE CHARACTERISTICS OF THE RECEIVER

	Conical scanner		Push-broom	
	NF	T_{rec}	NF	T_{rec}
C band	2.5 dB	226 K	3.5 dB	359 K
X band	2.5 dB	226 K	3.5 dB	359 K
Ku band	3.0 dB	290 K	4.0 dB	438 K

For both cases listed above, we have considered an FP overlap of ~30% both along track and across track to assure accurate sampling of the temperature scene on-ground and the values of B and T_{rec}, as shown in Tables I and II [7].

III. Reflector Antenna Design

To cover the required 600 km swath on the Earth surface, a beam scan about ±20° is needed. Due to high aberrations, stationary single-parabolic-reflector configurations are not suitable for such tasks. To solve this issue, one option is to consider a rotating reflector assembly as done for the SMAP mission [8], [9], but that goes at the cost of low integration time spent over an FP (thus low radiometric resolution ΔT_{min}) and increased complexity of the satellite platform, which must support mechanically rotating reflector system. Another option is to use a nonconventional toroidal reflector, which has already been investigated in late 80s with a cluster feed of horns [11]. Such a radiometer configuration is stationary and provides high radiometric sensitivity thanks to many simultaneous beams; however, a much more complex receiver must be implemented, comparing to the conical scan configuration.

We have investigated different reflector systems, including conventional offset parabolic reflectors with circular and elliptical apertures as the conical scanner, and toroidal single- and dual-reflector antennas for the push-broom concept.

The conical scan antenna is a conventional offset paraboloid with projected aperture D of 5 m and circular rim. The clearance is set to 1 m in order to provide space for the feed cluster and the focal length f is set to 3 m in order to make the design more compact.

The push-broom antenna is a torus reflector with projected aperture D of 5 m. The torus is obtained by rotating a section of a parabolic arc around a rotation axis. The focal length of the parabolic generator is also 5 m. A possible way of obtaining the torus is shown in Fig. 3: the feed axis is selected parallel to the rotation axis, implying that all feed element axes are parallel and orthogonal to the focal plane. The array feed becomes, therefore, planar, simplifying the mechanical and electrical design. The antenna shall be able to provide a scan of ±20° corresponding to a swath width of 600 km. The reflector rim is found by intersecting the torus surface by the

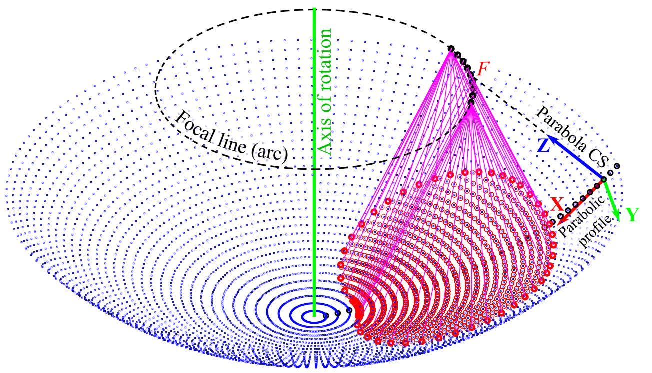

Fig. 3. Design procedure of a parabolic torus reflector (red surface): the parabolic profile (black circles at the bottom), defined in the coordinate system "Parabola CS" and with focal point F, is rotated around the green axis of rotation which itself is tilted with respect to the parabola axis. This transforms the profile focal point F to the focal line (arc) along which a PAF will be positioned. The arc angle defines the maximum beam scan angle and, correspondingly, the swath width.

feed cone up to the out-most scan positions of 20° and −20° (see [12, Fig. 3]). The antenna projected aperture is 5×7.5 m.

A more detailed explanation of the design procedure of the torus reflector can be found in [11].

IV. Limitations of Cluster Feeds of Horns

Cluster feeds for space-borne multifrequency radiometers are typically designed to provide a Gaussian-type beam with strong illumination taper toward the edge of the reflector (when seen in transmit situation) in order to maximize the antenna beam efficiency and minimize the sidelobe and cross-polarization power [30]. A typical example of such feeds is a conical horn antenna. This approach, however, leads to: 1) the lower spatial resolution due to the widening of the FP and 2) the difficulty to accommodate several feeds due to their large apertures, and hence several bands. Fig. 4(a)–(f) shows these limitations for the considered scanner and push-broom systems, respectively. As seen, P_{cross} of the scanner can only be minimized by employing a feed with the aperture diameter larger than 5λ and illumination taper that is <60 dB at 35°. This gives FP > 30 km and $D_c > 23$ km at the C-band, while FP $= 20$ km and $D_c = 5 - 15$ km are desired. The shortest D_c that can be achieved is ∼20 km, for which the realized P_{cross} is at least 3 times higher than the desired 0.34%. At higher frequency bands, realizing the required D_c is not a problem, as the sidelobe levels can be significantly reduced [see Fig. 6(c)] by underilluminating the reflector aperture, while providing FP $= 10$ km. However, the cross-polarization power is not acceptable.

For the push-broom system, the dependence of the radiometer characteristics from the illumination taper is similar to that of the scanner, and even larger feed apertures are needed due to the more shallow surface of the reflector. The main challenges for this system are attributed to the complex shape of the torus reflector and, as the result, more complex focal field [compare Fig. 5(a) and (b)]. The high coma-sidelobes and noncircular main lobe of the focal field distribution of the torus reflector [see Fig. 5(b)] cannot be accurately sampled by a single (horn) antenna feed, and this is the reason of the high sidelobe of the antenna far-field pattern [see Fig. 7(a)–(c)], and hence too large distance-to-coast. In contrast, dense FPAs are capable of handling these complexities, as will be demonstrated in Section V.

TABLE III
Number of Elements

	Conical scanner	Push-broom
Array grid	rectangular	polar
C band	$64 + 63 = 127$	$6 \times 111 \times 2 = 1332$
X band	$128 + 135 = 263$	$6 \times 153 \times 2 = 1836$
Ku band	$165 + 168 = 333$	$6 \times 255 \times 2 = 3060$

V. Dense Focal Plane Arrays

A. Array Models and Configurations

Based on the requirements derived in Section II, three FPAs of half-wavelength dipole antenna elements covering C-, X-, and Ku-bands have been designed for each radiometer. First, we computed the focal fields of several plane waves corresponding to the desired beam directions, and then used these to derive the minimum aperture sizes of FPAs and their positions in the focal regions, as shown in Fig. 5. After that, a parametric study was carried out to determine the minimum needed N_{el} and the corresponding interelement separation distance d_{el}. Note that to reduce the computational time, we have simplified the original MoM array model by assuming that all EEPs are identical to that of the central element (the validity of this assumption will be confirmed in Section V-D). The EEPs for each unique set of N_{el} and element positions were imported into the reflector antenna software GRASP10 to compute the secondary EEPs, which, in turn, were used to determine the optimum element excitation coefficients that will be discussed further. Table III summarizes the results of this parametric study. As one can see, for the conical scanner, we need 127, 263, and 333 antenna elements for the C-, X-, and Ku-bands, respectively, to provide 2, 21, and 30 beams. Since the radiometric resolution of the push-broom system is much higher (due to many more beams), as one can expect, this comes at the expenses of more elements. It is important to note that the required numbers of elements, determined through this optimization procedure, are almost twice smaller than when applying a conventional conjugate-field-matching optimization approach (see [12, Table 3]).

For both systems, the optimal d_{el} is near 0.75λ; this value satisfies the grating-lobe free condition [13] and also minimizes the active impedance variation of antenna elements due to their nonidentical excitation [31], [32].

B. Choice of the Array Radiating Element

The main requirements for the array radiating element are that: 1) it should be small enough to design the array with interelement spacing less than 0.75λ in order to avoid the grating lobes [13] and 2) it should be possible to use

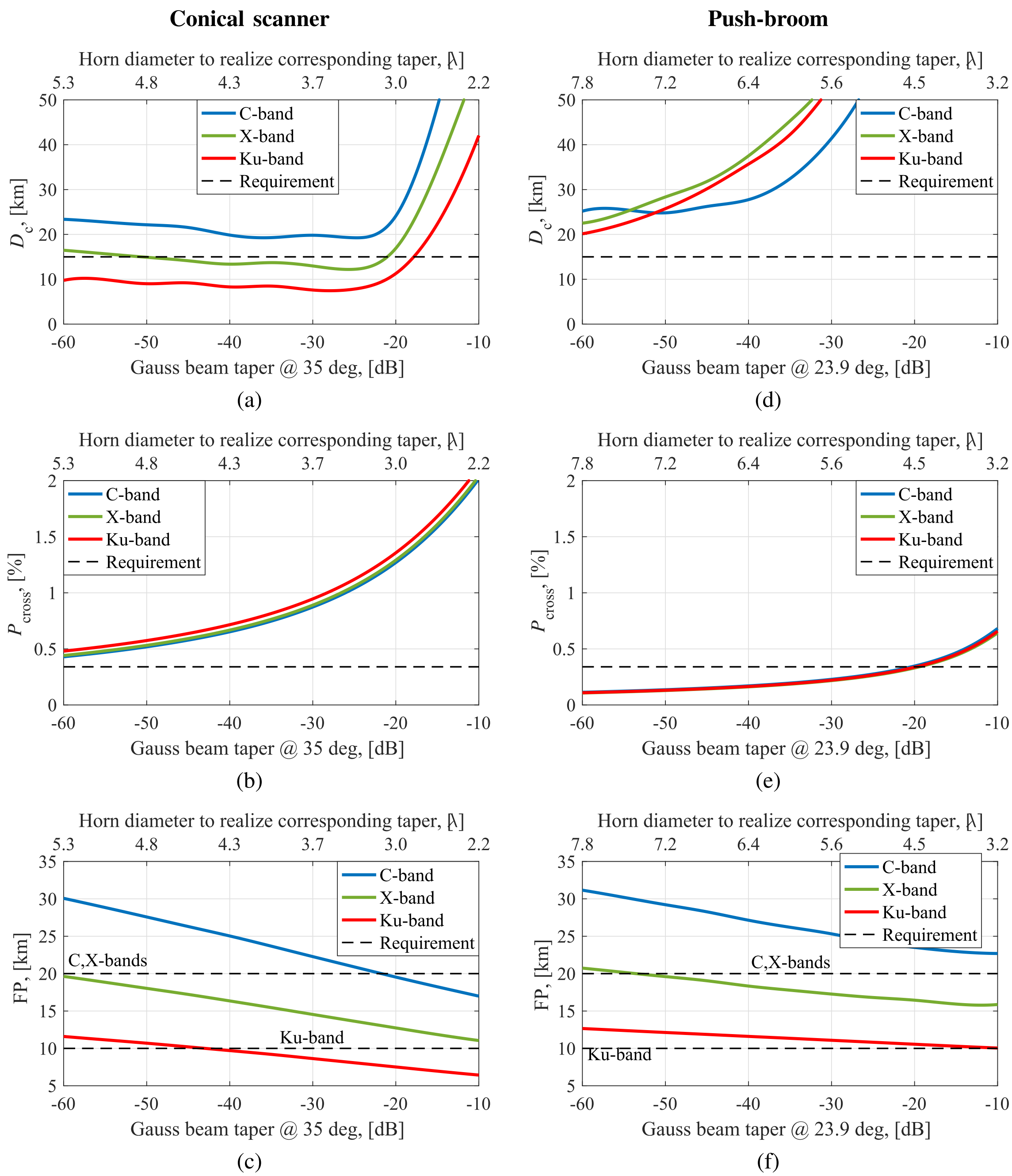

Fig. 4. Radiometer characteristics, i.e., the distance-to-land, relative cross-polarization power, and FP size, as the function of the illumination taper of the Gaussian feed for (a)–(c) conical scanner and (d)–(f) push-broom antenna configuration. The corresponding aperture diameter of the optimal circular horn [28], [29] is shown on the top axis.

in a dual-polarization configuration. Since the relative bandwidth required for the ocean remote sensing does not exceed 5 . . . 10%, it is not critical for element selection.

For arrays with the interelement spacing in the order of half wavelength, the optimal number of elements has been found weakly dependent from the element type, but primarily set by the following:

1) element excitation coefficients [33];
2) area of the array aperture, which depends on the focal field power region to be intercepted by the array feed for meeting the beam requirements [13];
3) interelement spacing in the array, which should be small enough for the accurate focal field sampling [13].

Other practical implementation requirements include a good impedance match between the antenna elements and amplifiers to minimize the receiver noise, robust and low weight space-qualified design.

For the purpose of this paper, i.e., to investigate different reflector systems at several frequency bands, it is sufficient to consider a simple half-wavelength dipole element when evaluating a complete set of radiation patterns and radiometer characteristics. For cross comparison, we will show some selected results for the push-broom antenna at the X-band for three different element types, which are: 1) a half-wavelength dipole antenna; 2) RUAG's patch-excited cup [34]; and 3) a Vivaldi antenna [35]. These results are summarized in Table IV, which

TABLE IV

COMPARISON OF THREE RADIATING ELEMENTS: CUTS OF THE EEP OF THE PAF CENTRAL ELEMENT, OPTIMAL EXCITATION COEFFICIENTS OF THE ARRAY ELEMENTS, AND CORRESPONDING RADIOMETER CHARACTERISTICS. THE RESULTS ARE FOR THE PUSH-BROOM SYSTEM AT THE C-BAND[1]

Characteristic	**Requirement**	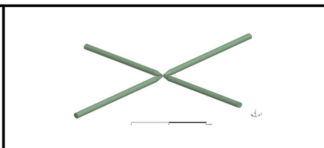		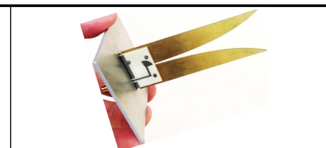
Embedded element pattern cuts of the PAF central element: —— Co-polar, E-plane; —— Co-polar, H-plane; - - - Cross-polar, D-plane; subtended angle of the push-broom reflector		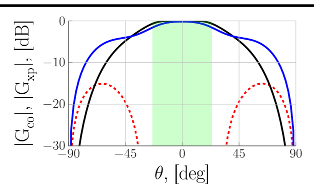	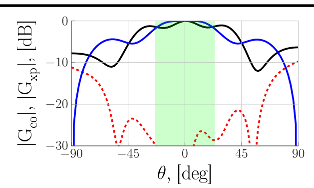	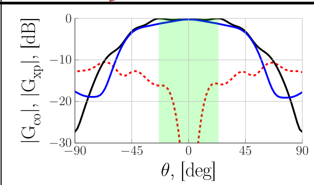
Excitation coefficients of co-polarized sub-array elements, [dB]		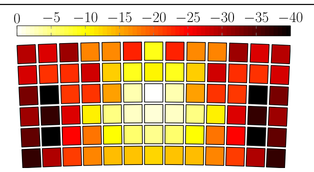	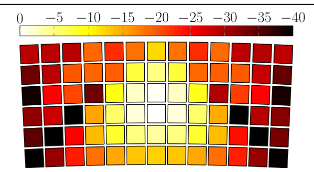	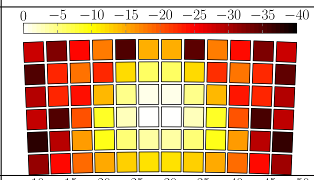
Excitation coefficients of cross-polarized sub-array elements, [dB]		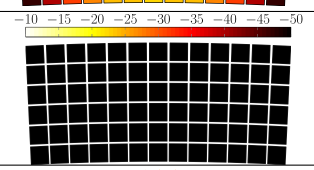	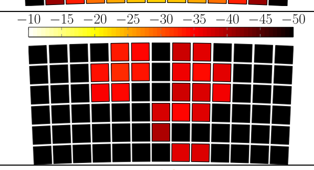	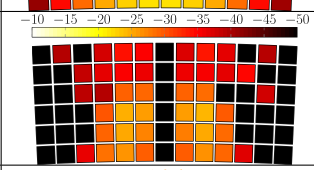
Distance to land, [km]	< 15	15.5	15.2	16.6
Rel. cross-pol. power, [%]	< 0.34	0.18	0.16	0.10
Beam efficiency, [%]		98.3	98.3	98.3
Footprint, [km]	< 20	22.2	22.7	22.2
Footprint ellipticity		1.57	1.53	1.59

[1] The radiometer characteristics for the PAF of dipole elements are slightly different from the ones in Table V due to different selected parameters of the beamformer.

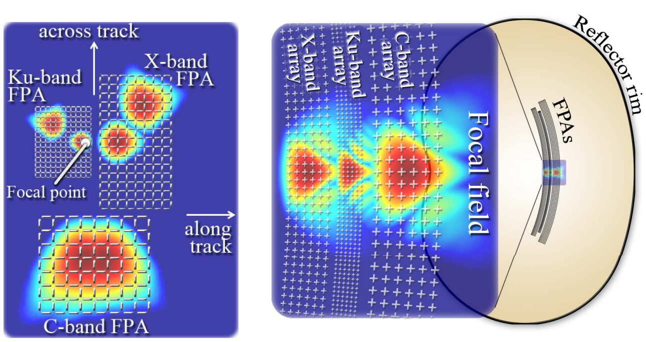

(a) (b)

Fig. 5. Example of focal field distributions due to multiple plane waves incident on (a) conical scan reflector antenna and (b) torus reflector antenna at the C-, X-, and Ku-bands, as calculated using the Physical Optics software GRASP10. For each frequency band, the array layout is overlaid above one (for push broom) or two (for conical scanner) focal field distributions.

include: 1) EEP cuts of the FPA central element; 2) the optimal excitation coefficients of copolarized and cross-polarized array elements; and 3) corresponding radiometer characteristics.

It is interesting to observe that despite the fact that all the element types have different EEPs (especially for the cross-polarization field component), the values of predicted radiometer characteristics differ insignificantly. The reason for that is the capability of the beamformer to compensate for these differences in the patterns.

Another interesting observation can be made about the cross-polarization power for each radiating element. Despite the cross-polarization level within the reflector, subtended angle is the lowest for the PAF of dipole elements and the largest for the Vivaldi PAF (see the EEPs in Table IV), the power contained in the cross-polarized field component after beamforming behaves in the opposite way, i.e., it is the smallest for the Vivaldi PAF (see "Rel. cross-pol. power" row in Table IV). This can be explained by the capability of the beamformer to use orthogonal array elements to compensate for the cross-polarized component of the secondary field, which is generated by the array elements and reflector itself. This can be seen from the excitation coefficients, where the cross-polarized elements are most strongly excited for the Vivaldi array.

C. Optimization Procedure for Element Excitation

In Section II, it has been shown that the antenna far-field beam should contain 99.72% of the total power within a circular cone with half-angle θ_c to realize the desired D_c. The goal is, therefore, to determine the excitation coefficients such that the angle θ_c becomes as small as possible, i.e., D_c is minimized.

The far field from the reflector antenna can be written as

$$\boldsymbol{E}_{\mathrm{far}}(\theta,\phi) = \sum_{i=1}^{N_{\mathrm{el}}} \alpha_i \boldsymbol{E}_{\mathrm{far},i}(\theta,\phi) \tag{9}$$

where $\boldsymbol{E}_{\mathrm{far},i}$ is the field due to element i, N_{el} is the total number of elements, and α_i is the corresponding complex

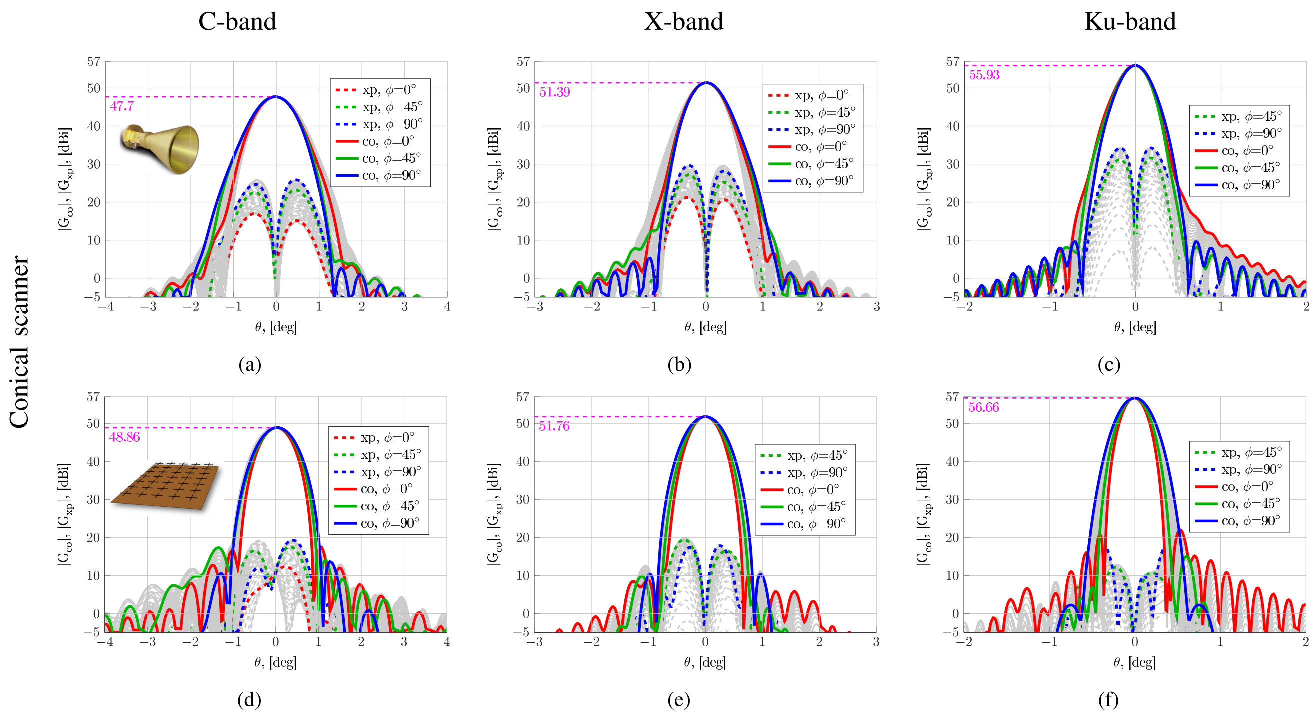

Fig. 6. Far-field pattern cuts for the conical scanner antenna at (a) and (d) C-band, (b) and (e) X-band, and (c) and (f) Ku-band, when the feed is (a)–(c) the Gaussian horn feed illuminating the reflector edge with the taper -30 dB, and (d)–(f) FPA with the optimum beamforming. The gray lines denote θ-cuts for ϕ varying from 0° to 180° with step 2.5°.

excitation coefficient. The radiated power within the cone of half-angle θ_c can be written as

$$P_c(\theta_c) = \int_0^{2\pi} \int_0^{\theta_c} |\boldsymbol{E}_{\text{far}}(\theta, \phi)|^2 \sin\theta \, \mathrm{d}\theta \, \mathrm{d}\phi. \tag{10}$$

If the expression (9) is inserted in (10), it is seen that it becomes a quadratic polynomial in the α_i variables and can be written in the form

$$P_c(\theta_c) = \boldsymbol{\alpha}^H \mathbf{A} \boldsymbol{\alpha} \tag{11}$$

where $\boldsymbol{\alpha} = [\alpha_1, \alpha_2, \ldots, \alpha_N]^T$ and H is the Hermitian operator. The matrix $\mathbf{A}$ is Hermitian of size $N_{\text{el}} \times N_{\text{el}}$ such that the expression in (11) becomes a real number. Note that the matrix $\mathbf{A}$ is a function of θ_c.

The power $P_c(\theta_c)$ in (10) must be related to the total radiated power from the feed array. This power, P_{tot}, can be computed from the expression (10) if θ_c is replaced by $\pi/2$ and the reflector patterns $\boldsymbol{E}_{\text{far},i}$ are replaced by the array element patterns $\boldsymbol{E}_{\text{far,array},i}$. Again the power P_{tot} becomes a quadratic polynomial in the variables $\boldsymbol{\alpha}$ such that

$$P_{\text{tot}} = \boldsymbol{\alpha}^H \mathbf{C} \boldsymbol{\alpha}. \tag{12}$$

For a given value of θ_c, it is thus desired to find the excitations $\boldsymbol{\alpha}$ that maximize the ratio

$$\frac{P_c(\theta_c)}{P_{\text{tot}}} = \frac{\boldsymbol{\alpha}^H \mathbf{A} \boldsymbol{\alpha}}{\boldsymbol{\alpha}^H \mathbf{C} \boldsymbol{\alpha}}. \tag{13}$$

It can be shown that the maximum value of this ratio is the maximum eigenvalue λ of the expression

$$\mathbf{A} \boldsymbol{\alpha} = \lambda \mathbf{C} \boldsymbol{\alpha} \tag{14}$$

and that the vector holding the complex excitation coefficients is given by the corresponding eigenvector.

The present optimization method is similar to the one reported in [14]—which is based on a more general signal-to-noise-ratio algorithm—but simpler to implement. Since for the considered application scenario, the optimization is strongly driven by the acceptable sidelobe and cross-polarization power of the antenna, and the radiometric performances obtained by the two algorithms are very similar.

D. Antenna Patterns and Radiometric Characteristics

Dense FPAs offer more degrees of freedom in beamforming, as compared to conventional feeds, and thereby can provide highly optimized beams with more circular-symmetric main lobes and much lower cross polarization and sidelobe levels, as shown in Figs. 6(d)–(f) and 7(d)–(f). This results in significantly better radiometric characteristics for both systems. As one can see in Table V, the realized D_c of the conical scanner is 6.6–14 km and P_{cross} is only 0.10%–0.15% (i.e., about one order of magnitude better than for the horn feed); for the push-broom radiometer, the respective quantities are less than 16 km (while the horn feed cannot fulfill this requirement) and 0.08%–0.12% (i.e., three times better than the horn feed). Furthermore, the latter system has wide scan-range performance, where the characteristics of all multiple beams within the angular range of ±20° are virtually identical, thanks to the symmetry of the torus reflector in the azimuthal plane and the moon-like shape of the FPA that matches the focal line of the reflector [see Fig. 5(b)].

The accuracy of the above analysis (that is based on the assumption of identical array element patterns) has been evaluated by cross-comparing the antenna patterns and corresponding radiometric characteristics with those obtained through the full MoM model. Fig. 8 shows the results for

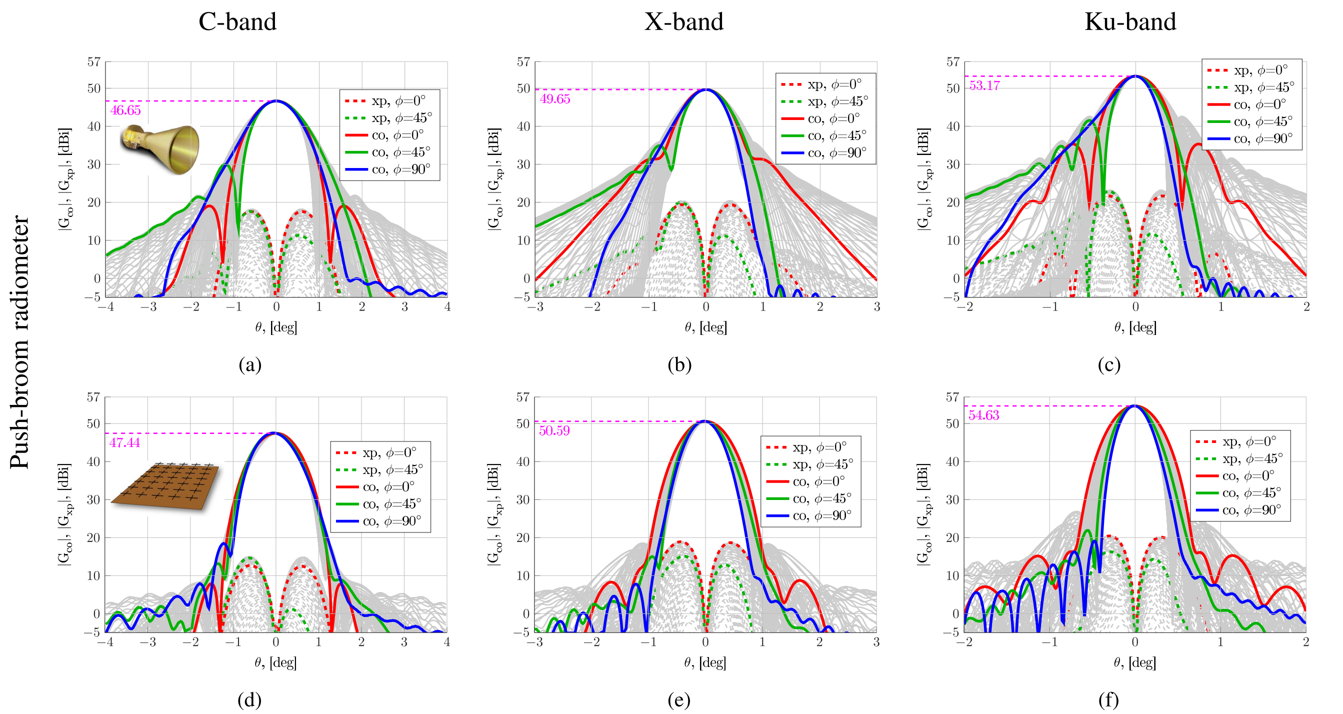

Fig. 7. Far-field pattern cuts for the push-broom radiometer antenna at (a) and (d) C-band, (b) and (e) X-band, and (c) and (f) Ku-band, when the feed is (a)–(c) Gaussian horn feed illuminating the reflector edge with the taper −30 dB, and (d)–(f) FPA with the optimum beamforming. The gray lines denote θ-cuts for ϕ varying from 0° to 180° with step 2.5°.

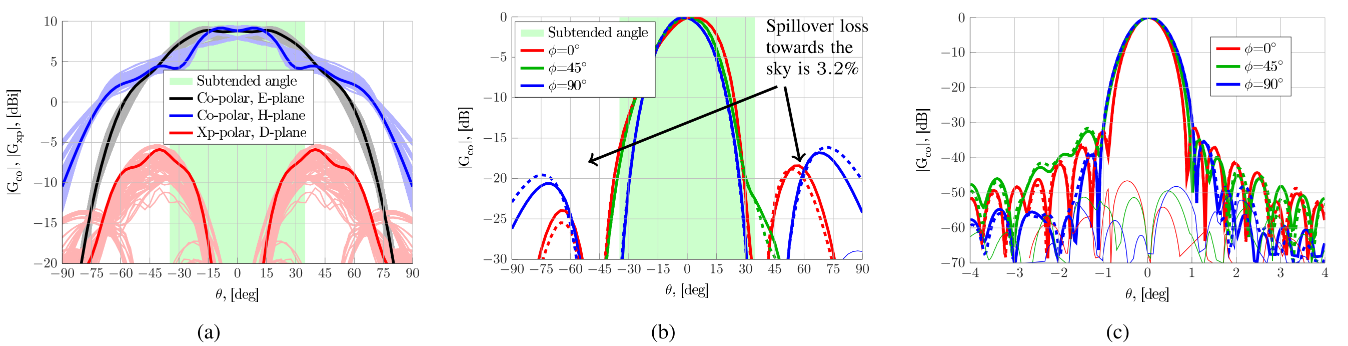

Fig. 8. (a) All EEPs of the C-band FPA for the conical scanner at E-, H- and D-planes, as obtained through the MoM in CAESAR software [36], where the bold lines correspond to the central antenna element of the array. (b) Beamformed far-field pattern cuts of the FPA within the reflector subtended angle region for the conical scan antenna. (c) Far-field pattern cuts of the reflector antenna for beam 1. Solid lines: MoM array model. Dashed lines: model with the assumed identical EEPs of the array. Thin solid lines: relative normalized difference between the antenna patterns obtained with the above models.

the C-band, as the worse-case scenario among the considered ones. As seen, the relative difference between the far-field patterns obtained with the simplified and more rigorous FPA models is negligible, so as the difference between the corresponding sets of radiometric characteristics (see Table V). This observation might appear counterintuitive, given a significant variation between the EEPs of the array, as shown in Fig. 8(a). However, one should realize that the optimal pattern of the feed leading to the minimum distance to land represents a combined effect of the EEPs and element excitation coefficients. Hence, when the optimization algorithm is applied to the set of nonidentical EEPs, the excitation coefficients are modified with respect to that determined for the identical EEP case. For the considered arrays with more than 100 dipole antenna elements, the resultant optimal feed patterns have been found very similar for both array models [see the example for C-band in Fig. 8(b) and (c)]. This observation, however, may not be valid for arrays with fewer and denser-spaced elements.

VI. Receiver Considerations

In this section, we briefly consider receiver resource requirements in order to see if implementation of the present antenna concept is feasible and realistic. We consider the receiver where the signals from different antenna elements contribute to more than one beam, and each antenna element is connected to its own receiver, followed by an A/D converter. The beamforming process takes place in a field programmable gate array (FPGA), using complex digital multipliers and adders. Both the scanner and the push-broom system require a large number of elements to fulfill the radiometric requirements. Hence, resource requirements concerning the size, mass, and especially power consumption are important issues.

TABLE V

RADIOMETRIC CHARACTERISTICS OF THE CONICAL SCANNER AND PUSH-BROOM SYSTEMS FOR THE GAUSSIAN HORN AND FPA. THE VALUES IN BRACKETS ARE FOR THE FULL MOM ARRAY MODEL, AND THE OTHER VALUES ARE WHEN ASSUMING IDENTICAL EEPS

Radiometer characteristic	Require-ment	Conical scanner			Push-broom	
		Horn feed	FPA		Horn feed	FPA
			Beam 1	Beam 2		
C-band						
Distance to land, [km]	<15	19.2	14.2 (14.2)	14.2 (14.2)	41.4	16.1
Rel. cross-pol. power, [%]	<0.34	1.04	0.15 (0.06)	0.10 (0.07)	0.23	0.08
Beam efficiency, [%]		97.2	95.6 (96.0)	95.6 (96.0)	96.1	97.8
Footprint, [km]	<20	21	19.6 (19.6)	19.6 (19.6)	25.3	23.1
Footprint ellipticity		1.64	1.43 (1.44)	1.44 (1.44)	1.57	1.48
X-band						
Distance to land, [km]	<15	13.0	9.7	9.8	55.3	13.4
Rel. cross-pol. power, [%]	<0.34	0.89	0.10	0.10	0.22	0.12
Beam efficiency, [%]		97.7	98.2	97.4	95.0	98.4
Footprint, [km]	<20	14.5	14.2	14.2	17.3	15.9
Footprint ellipticity		1.64	1.32	1.38	1.48	1.21
Ku-band						
Distance to land, [km]	<15	7.6	6.6	6.6	53.2	13.4
Rel. cross-pol. power, [%]	<0.34	0.95	0.03	0.07	0.22	0.08
Beam efficiency, [%]		97.7	97.4	97.2	84.5	98.0
Footprint, [km]	<10	8.6	8.0	8.2	11.1	10.0
Footprint ellipticity		1.67	1.24	1.35	1.27	1.05

A study of the state-of-the-art microwave components, assuming a superheterodyne receiver (see [37, Fig. 7]), has been carried out. It has been found that at the considered frequency bands, most components are small and lightweight, and thus volume and mass are not deemed to be a problematic issue. Power consumption has dropped dramatically over the past decade, and 1 W per receiver is now a realistic estimate. Furthermore, the output signals from FPA elements have to be optimally combined in a dedicated beamforming network to form the desired antenna beams. This involves a number of FPGAs and the average power consumption is estimated to be 0.24 W per receiver. Future radiometers must include intelligent radio frequency interference (RFI) detection and mitigation processors. Based on a representative case study of such a processor [38], the power consumption can be estimated to be 0.14 W per receiver.

In summary, the power estimate is: $1+0.24+0.14 = 1.38$ W per receiver, using present state-of-the-art components. The total number of receivers is 6228 in the push-broom case. This results in a total power consumption of 8.6 kW, which is not realistic today. For the scanner with 723 receivers, the estimate is 1000 W—a large number, but feasible.

This paper is a preparation for the future, and it is of interest to base a power budget on realistic developments over a five-year time frame. Already now, A/D converters able to subsample signals up to X-band are available in research labs, and within very few years, the Ku-band is also possible. Thus, we do not need the superheterodyne layout, and the local oscillator and its power consumption can be avoided. The new, fast A/D converters use very small signal levels typically around -35 dBm, and hence not much gain is needed in the receiver (also saving on power). The development concerning amplifier power consumption is also impressive. For global power budget estimates, we can within a few years assume $\sim$35 mW per receiver. If we assume a similar reduction for processing circuitry, the result is 9 mW for the beamforming network, and 5 mW for the RFI processor, i.e., 49 mW per receiver. For the push-broom system, this amounts to a total power consumption of 305 W, which is certainly realistic. For the scanner, the estimate is about 35 W.

VII. CONCLUSION

Existing space-borne microwave radiometers that are used for the assessment of ocean parameters like salinity, temperature, and wind can provide valid observations only up to $\sim$100 km from the coastline, and hence do not allow for monitoring of the coastal areas and ice-edge polar seas and measuring under extreme wind and weather conditions. To achieve the desired precision, as required for future missions, we propose digitally beamforming dense focal plane arrays (FPAs)—previously not used in space-borne applications—employed either in a traditional conical-scan offset parabolic reflector antenna or in a wide-scan torus reflector system.

When synthesized and excited according to the proposed optimum beamforming procedure—aiming to minimize the signal contamination given by the sidelobes and cross polarization of antenna beams covering the land—the number of the FPA antenna elements and associated receivers can be kept to minimum. In this procedure, the input parameters include the number of array elements, their positions, and the secondary EEPs, which are computed after the illumination of the reflector antenna, and the output parameters are the optimal complex-valued element excitations. Although the primary EEPs are generally not identical, due to the array antenna mutual coupling and edge truncation effects, for the considered FPAs with more than 100 dipole antenna elements and interelement spacing of 0.75λ, it has been found sufficient to use a single primary EEP, i.e., the one for a central element of the array, as the source of the secondary EEPs for all elements in order to accurately predict the achievable radiometric characteristics.

For both types of radiometers, the realized resolutions are at least twice higher than the values provided by the current systems, and the distance to coastline is as short as 6–15 km.

This excellent performance was shown to be impossible with traditional multifrequency FPAs of horns in one-horn-per-beam configuration, as these cannot compensate for the high cross polarization of off-axis beams in conical scanners, and produce unacceptably high sidelobes due to severe focal-field undersampling effects in torus reflector systems.

Our analysis of realistic developments of digital processors predicts acceptable receiver resources budget for such multi-beam radiometers within a five-year time frame.

The future work will address space-qualified array design and possible reduction of the array elements to minimize power consumption.

Acknowledgment

The authors would like to thank J. Wettergren and S. S. Kildal from RUAG Space, Sweden, for providing us with the data for the patch-excited cup antenna.

References

[1] C. Prigent *et al.*, "Analysis of the potential and limitations of microwave radiometry for the retrieval of sea surface temperature: Definition of MICROWAT, a new mission concept," *Geophys. Res. Oceans*, vol. 118, no. 6, pp. 3074–3086, Jun. 2013.

[2] E. V. Zabolotskikh, L. M. Mitnik, and B. Chapron, "New approach for severe marine weather study using satellite passive microwave sensing," *Geophys. Res. Lett.*, vol. 40, no. 13, pp. 3347–3350, Jul. 2013.

[3] N. Reul, B. Chapron, T. Lee, C. Donlon, J. Boutin, and G. Alory, "Sea surface salinity structure of the meandering Gulf stream revealed by SMOS sensor," *Geophys. Res. Lett.*, vol. 41, no. 9, pp. 3141–3148, May 2014.

[4] *High Resolution Microwave Wind and Temperature (MICROWAT)*. Accessed: Nov. 15, 2017. [Online]. Available: http://due.esrin.esa.int/stse/page_stse_project134.php

[5] P. W. Gaiser, "The WindSat spaceborne polarimetric microwave radiometer: Sensor description and early orbit performance," *IEEE Trans. Geosci. Remote Sens.*, vol. 42, no. 11, pp. 2347–2361, Nov. 2004.

[6] *The Advanced Microwave Scanning Radiometer—Earth Observing System (AMSR-E)*. Accessed: Nov. 15, 2017. [Online]. Available: http://nsidc.org/data/NSIDC-0301

[7] N. Skou and D. L. Vine, *Microwave Radiometer Systems: Design & Analysis*. Norwood, MA, USA: Artech House, 2006.

[8] M. Mobrem, E. Keay, G. Marks, and E. Slimko, "Development of the large aperture reflector/boom assembly for the SMAP spacecraft," in *Proc. ESA/ESTEC Workshop Large Deployable Antennas*, Noordwijk, The Netherlands, Oct. 2012.

[9] *SMAP Handbook—Soil Moisture Active Passive*. Accessed: Nov. 15, 2017. [Online]. Available: https://smap.jpl.nasa.gov/system/internal_resources/details/original/178_SMAP_Handbook_FINAL_1_JULY_2014_Web.pdf

[10] R. A. Hoferer and Y. Rahmat-Samii, "RF characterization of an inflatable parabolic torus reflector antenna for space-borne applications," *IEEE Trans. Antennas Propag.*, vol. 46, no. 10, pp. 1449–1457, Oct. 1998.

[11] P. H. Nielsen, K. Pontoppidan, J. Heeboell, and B. Le Stradic, "Design, manufacture and test of a pushbroom radiometer," in *Proc. 6th Int. Conf. Antennas Propag. (ICAP)*, Coventry, U.K., Apr. 1989, pp. 126–130.

[12] C. Cappellin *et al.*, "Novel multi-beam radiometers for accurate ocean surveillance," in *Proc. 8th Eur. Conf. Antennas Propag. (EuCAP)*, The Hague, The Netherlands, Apr. 2014, pp. 3531–3535.

[13] O. A. Iupikov *et al.*, "Dense focal plane arrays for pushbroom satellite radiometers," in *Proc. 8th Eur. Conf. Antennas Propag. (EuCAP)*, The Hague, The Netherlands, Apr. 2014, pp. 3536–3540.

[14] O. A. Iupikov *et al.*, "An optimal beamforming algorithm for phased-array antennas used in multi-beam spaceborne radiometers," in *Proc. 9th Eur. Conf. Antennas Propag. (EuCAP)*, Lisbon, Portugal, Apr. 2015, pp. 1–5.

[15] C. Cappellin *et al.*, "Design of a push-broom multi-beam radiometer for future ocean observations," in *Proc. 9th Eur. Conf. Antennas Propag. (EuCAP)*, Lisbon, Portugal, Apr. 2015, pp. 1–5.

[16] J. R. Fisher and R. F. Bradley, "Full-sampling array feeds for radio telescopes," *Proc. SPIE*, vol. 4015, pp. 308–318, Jul. 2000.

[17] K. F. Warnick *et al.*, "Towards a high sensitivity cryogenic phased array feed antenna for the Green Bank Telescope," in *Proc. 30th URSI Gen. Assembly Sci. Symp.*, Istanbul, Turkey, Aug. 2011, pp. 1–4.

[18] D. R. DeBoer *et al.*, "Australian SKA pathfinder: A high-dynamic range wide-field of view survey telescope," *Proc. IEEE*, vol. 97, no. 8, pp. 1507–1521, Aug. 2009.

[19] B. Veidt, T. Burgess, R. Messing, G. Hovey, and R. Smegal, "The DRAO phased array feed demonstrator: Recent results," in *Proc. 13th Int. Symp. Antenna Technol. Appl. Electromagn. Can. Radio Sci. Meet. (ANTEM/URSI)*, Banff, AB, Canada, Feb. 2009, pp. 1–4.

[20] M. V. Ivashina, O. Iupikov, R. Maaskant, W. A. van Cappellen, and T. Oosterloo, "An optimal beamforming strategy for wide-field surveys with phased-array-fed reflector antennas," *IEEE Trans. Antennas Propag.*, vol. 59, no. 6, pp. 1864–1875, Jun. 2011.

[21] Y. Wu, X. Zhang, B. Du, C. Jin, L. Zhang, and K. Zhu, "Design of antenna array for the L-band phased array feed for FAST," in *Proc. Int. Symp. Antennas Propag. (ISAP)*, Nanjing, China, Oct. 2013, pp. 11–13.

[22] K. F. Warnick, R. Maaskant, M. V. Ivashina, D. B. Davidson, and B. D. Jeffs, "High-sensitivity phased array receivers for radio astronomy," *Proc. IEEE*, vol. 104, no. 3, pp. 607–622, Mar. 2016.

[23] (2017). *Boeing: Satellite Development Center—Geo-Mobile—Thuraya-2, 3*. Accessed: Nov. 15, 2017. [Online]. Available: http://web.archive.org/web/20120509231723/http://www.boeing.com/defensespace/space/bss/factsheets/geomobile/thuraya2_3/thuraya2_3.html

[24] (2017). *Inmarsat—Our Satellites*. Accessed: Nov. 15, 2017. [Online]. Available: https://www.inmarsat.com/about-us/our-satellites/

[25] M. Schneider, C. Hartwanger, E. Sommer, and H. Wolf, "The multiple spot beam antenna project 'Medusa,'" in *Proc. Eur. Conf. Antennas Propag. (EuCAP)*, Berlin, Germany, Mar. 2009, pp. 726–729.

[26] M. Schneider, C. Hartwanger, and H. Wolf, "Antennas for multiple spot beam satellites," *CEAS Space J.*, vol. 2, nos. 1–4, pp. 59–66, Dec. 2011.

[27] P. Bosshard *et al.*, "Thales alenia space HTS/V-HTS multiple beam antennas sub-systems on the right track," in *Proc. 10th Eur. Conf. Antennas Propag. (EuCAP)*, Davos, Switzerland, Apr. 2016, pp. 1–5.

[28] T. Teshirogi and T. Yoneyama, *Modern Millimeter-wave Technologies*. Amsterdam, The Netherlands: IOS Press, 2001.

[29] P.-S. Kildal, *Foundations of Antenna Engineering—A Unified Approach for Line-of-Sight and Multipath*. Gothenburg, Sweden: Kildal Antenn AB, 2015. [Online]. Available: http://www.kildal.se/download-book/

[30] S. Contu and F. M. Marinelli, "The antenna system for the multifrequency imaging microwave radiometer: M.I.M.R," in *Antennas Propag. Soc. Int. Symp. AP-S. Dig.*, vol. 3. Seattle, WA, USA, Jun. 1994, pp. 2054–2057.

[31] M. Arts, M. Ivashina, O. Iupikov, L. Bakker, and R. van den Brink, "Design of a low-loss low-noise tapered slot phased array feed for reflector antennas," in *Proc. 4th Eur. Conf. Antennas Propag.*, Barcelona, Spain, Apr. 2010, pp. 1–5.

[32] K. F. Warnick, D. Carter, T. Webb, J. Landon, M. Elmer, and B. D. Jeffs, "Design and characterization of an active impedance matched low-noise phased array feed," *IEEE Trans. Antennas Propag.*, vol. 59, no. 6, pp. 1876–1885, Jun. 2011.

[33] M. V. Ivashina, M. N. M. Kehn, P.-S. Kildal, and R. Maaskant, "Decoupling efficiency of a wideband Vivaldi focal plane array feeding a reflector antenna," *IEEE Trans. Antennas Propag.*, vol. 57, no. 2, pp. 373–382, Feb. 2009.

[34] J. Johansson and P. Ingvarson, "Array antenna activities at RUAG space: An overview," in *Proc. 7th Eur. Conf. Antennas Propag. (EuCAP)*, Gothenburg, Sweden, Apr. 2013, pp. 666–669.

[35] O. A. Iupikov, A. A. Roev, and M. V. Ivashina, "Prediction of far-field pattern characteristics of phased array fed reflector antennas by modeling only a small part of the array—Case study of spaceborne radiometer antennas," in *Proc. 11th Eur. Conf. Antennas Propag. (EUCAP)*, Paris, France, Mar. 2017, pp. 2636–2639.

[36] R. Maaskant, "Analysis of large antenna systems," Ph.D. dissertation, Dept. Elect. Eng., Eindhoven Univ. Technol., Eindhoven, The Netherlands, 2010. [Online]. Available: http://alexandria.tue.nl/extra2/201010409.pdf

[37] N. Skou *et al.*, "t Klooster, "Future spaceborne ocean missions using high sensitivity multiple-beam radiometers," in *Proc. IEEE Geosci. Remote Sens. Symp. (IGARSS)*, Quebec City, QC, Canada, Jul. 2014, pp. 2546–2549.

[38] N. Skou, S. S. Kristensen, A. Kovanen, and J. Lahtinen, "Processor breadboard for on-board RFI detection and mitigation in MetOp-SG radiometers," in *Proc. IEEE Int. Geosci. Remote Sens. Symp. (IGARSS)*, Milan, Italy, Jul. 2015, pp. 1445–1448.

Oleg A. Iupikov (S'12–M'16) received the M.Sc. degree (*cum laude*) in electrical engineering from Sevastopol National Technical University, Sevastopol, Ukraine, in 2006, and the Ph.D. degree from the Chalmers University of Technology, Gothenburg, Sweden, in 2017.

He was with the Radio Engineering Bureau, Sevastopol. During this period, he was also a Visiting Researcher with The Netherlands Institute for Radio Astronomy (ASTRON), Dwingeloo, The Netherlands, where he was involved in the development of the focal plane array simulation software for the APERTIF radio telescope. This visit was funded by the SKADS Marie Curie Visitor Grant and the APERTIF Project. He has authored/co-authored over 30 journal and conference papers. His current research interests include receiving antenna array systems, in particular focal plane arrays for radio astronomy and microwave remote sensing applications, numerical methods for their analysis and optimization, and signal processing algorithms for antenna systems.

Marianna V. Ivashina (M'11–SM'13) received the Ph.D. degree in electrical engineering from Sevastopol National Technical University, Sevastopol, Ukraine, in 2001.

From 2001 to 2010, she was with The Netherlands Institute for Radio Astronomy (ASTRON), Dwingeloo, The Netherlands, where she carried out research on innovative phased array technologies for future radio telescopes, such as the square kilometer array. She is currently a Professor in antenna systems with the Chalmers University of Technology, Gothenburg, Sweden. Her current research interests include wideband receiving arrays, antenna system modeling techniques, receiver noise characterization, signal processing for phased arrays, and radio astronomy. She has published extensively on the above topics, having authored/co-authored over 120 journal and conference papers.

Dr. Ivashina is currently an Associate Editor of the IEEE TRANSACTIONS ON ANTENNAS AND PROPAGATION.

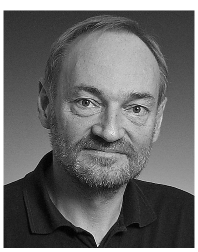

Niels Skou (S'78–M'79–SM'96–F'03) received the M.Sc., Ph.D., and D.Sc. degrees from the Technical University of Denmark, Kongens Lyngby, Denmark, in 1972, 1981, and 1990, respectively.

His research has been directed toward microwave remote sensing systems. After working for three years with the development of radar systems for measuring the ice sheets in Greenland and Antarctica, his interest turned toward microwave radiometry. He developed a scanning, multifrequency, airborne radiometer system. After that, his subjects were radiometer measurements of sea ice and oil pollution on the sea, spaceborne radiometer systems, and development of new systems for specific purposes. In the mid-1980s, his interest turned back to active instruments and he became involved in the development of an airborne, multifrequency, polarimetric, and interferometric synthetic aperture radar system with special emphasis on calibration fidelity. However, activity within microwave radiometry has continued, mainly within the areas of synthetic aperture radiometry and polarimetric radiometry. The work on synthetic aperture radiometry has led to the European Space Agency's Soil Moisture and Ocean Salinity (SMOS) Mission, Noordwijk, The Netherlands, and he was a member of the SMOS Science Advisory Group. In support of SMOS, a range of airborne campaigns with L-band radiometers have been carried out over land, sea, Arctic sea ice, and the East Antarctica Dome-C. He has taken a special interest in radio frequency interference (RFI), using digital signal processing and polarimetry to detect and mitigate harmful RFI. He is currently a Professor with the Technical University of Denmark. He is also a member of the Quality Working Group. His current research interests include development of a real-time RFI processor and the design of very small receiver systems for focal plane arrays, both to be used in the next generation of spaceborne radiometers.

Cecilia Cappellin received the M.Sc. degree in telecommunication engineering from the University of Siena, Siena, Italy, in 2004, and the industrial Ph.D. degree from the Technical University of Denmark, Kongens Lyngby, Denmark, in 2007.

She joined TICRA, Copenhagen, Denmark, in 2004. After the completion of the Ph.D. in 2007, she has worked on numerous ESA contracts, like in-orbit reconfigurable shaped reflectors, advanced multi-beam radiometers and large mesh reflectors with grating lobe reduction, as well as scattering analysis and reflector and feed antenna designs for customers. Since 2010 she is the manager of TICRA's consultancy division. She is responsible for, and deeply involved in, TICRA's software support and software training, analysis and design of antenna systems as well as internally funded R&D projects. As part of the consultancy division, she actively participates in the test and development cycle of all TICRA software products.

Knud Pontoppidan received the M.Sc.E.E. and Ph.D. degrees from the Technical University of Denmark, Kongens Lyngby, Denmark, in 1965 and 1972, respectively.

He joined TICRA, Copenhagen, Denmark, in 1972. Since then, he has been involved in radio telescopes, deployable reflector antennas and contoured beam antennas, omnidirectional or near-anisotropic antennas, physical optics, and the geometrical theory of diffraction. He has by now 45 years of experience in reflector antenna analysis and design. A large effort has been devoted to the influence of reflector tolerances and reflector electrical properties. He has been the Project Manager and technical responsible of uncountable ESA contracts and antenna designs. He has also been involved in the design and analysis of compact test ranges. Within this field, he has especially investigated the coupling between the range and the antenna under test. He has been the initiator of a study on reconfigurable reflectors made by piano wires net, investigating the mechanical, and electrical and mathematical properties of the reconfigurable net. He has developed significant parts of the GRASP software. He is among the best experts of the software, providing continuous support to TICRA's customers on all TICRA's software packages.

Cornelis G. M. (Kees) van 't Klooster (M'81–SM'88) received the IR degree in electrical engineering from the Eindhoven University of Technology, Eindhoven, The Netherlands, in 1978, and the M.Sc. degree in space system engineering from Delft University of Technology, Delft, The Netherlands, in 2001.

In 1978, he joined the Physics Laboratory, Toegepast Natuurkundig Onderzoek, The Hague, The Netherlands, as an Antenna Engineer, and was involved in ferrite phase shifters, waveguide based phased array antennas, and planar near-field testing. In 1984, he joined the European Space Agency (ESA) in the Technical Directorate, where he was involved in antennas for satellite projects (remote sensing and scientific), including Meteosat, European Remote Sensing Satellite (ERS), and a few other satellites. He was responsible for research and development contract studies on slotted waveguide antennas, feeds and feed-arrays, SAR and radiometer antennas, antenna testing, and took part in studies on large deployable antennas. He has authored or co-authored over 150 papers. Achievements include initiation of dedicated new panel technology for Atacama Large Millimeter/Submillimeter Array with industry, Media Lario, Bosisio Parini, Italy. as a spin-off from an X-ray telescope space technology and initiation of investigations with the institute Joint Institute for Very Long Baseline Interferometry (VLBI) in Europe (JIVE) into VLBI tracking of the Huygens probe during its landing on Titan. The latter work has been realized by JIVE. After retirement in 2015, he continues part time with antenna activities in universities and some consultancies.

He received the ESA Douglash Marsh Fellowship for one year in Moscow at the Lebedev Physical Institute within the Radio-Astron Space-VLBI Project Team.